Available online at www.sciencedirect.com
ScienceDirect
European Journal of Mechanics B/Fluids 27 (2008) 75–95

A priori evaluations and least-squares optimizations of turbulence models for fully developed rotating turbulent channel flow

Olof Grundestam *, Stefan Wallin, Arne V. Johansson

Department of Mechanics, Royal Institute of Technology, KTH SE-100 44 Stockholm, Sweden

Received 16 May 2006; received in revised form 12 December 2006; accepted 1 March 2007

Available online 14 March 2007

Abstract

The present study involves a priori tests of pressure-strain and dissipation rate tensor models using data from direct numerical simulations (DNS) of fully developed turbulent channel flow with and without spanwise system rotation. Three different pressure-strain rate models are tested ranging from a simple quasi-linear model to a realizable fourth order model. The evaluations demonstrate the difficulties of developing RANS-models that accurately describe the flow for a wide range of rotation numbers. Furthermore, least-squares based tensor representations of the exact pressure-strain and dissipation rate tensors are derived pointwise in space. The relation obtained for the rapid pressure-strain rate is exact for general 2D mean flows. Hence, the corresponding distribution of the optimized coefficients show the ideal behaviour. The corresponding representations for the slow pressure-strain and dissipation rate tensors are incomplete but still optimal in a least-squares sense. On basis of the least-squares analysis it is argued that the part of the representation that is tensorially linear in the Reynolds stress anisotropy is the most important for these parts.

Keywords: A priori testing; Turbulence model; Least-squares method; Channel flow

1. Introduction

The assessment of Reynolds averaged Navier–Stokes (RANS) based turbulence closures is usually presented in the form of flow predictions for a number of different test cases using the complete proposed turbulence closure. An interesting complement to this kind of investigations is a priori tests. In an a priori test a specific part of a model is evaluated by using flow data from a direct numerical simulation (DNS) and then, of course, compared to the corresponding correlation evaluated from the DNS. In this way, detailed information can be obtained about how accurately a particular model (or part of a model) approximates the corresponding exact physical term under given flow conditions. The need for accurate and complete flow data limits a priori testing to flows that can be studied with DNS. Fortunately the number of flows for which DNS is applicable have grown due to increased computational capacity and today, DNS-data is available for, e.g., turbulent channel flow with and without rotation, turbulent rotating pipe flow as well as boundary layer flows with various pressure gradients. Large eddy simulations (LES) can provide

* Corresponding author.
E-mail addresses: olof@mech.kth.se (O. Grundestam), stefan.wallin@foi.se (S. Wallin), viktor@mech.kth.se (A.V. Johansson).

0997-7546/$ – see front matter
doi:10.1016/j.euromechflu.2007.03.001

data in flows where the computational cost of DNS is too high. LES, however, gives flow data that to some extent depend on the accuracy of the sub-grid scale model.

In RANS related modelling, closure calibration is often performed by tuning the model parameters such that the overall model predictions, for typically a few generic flows, are in as good agreement as possible with a DNS or an experiment. Whereas this approach is no worse than any other in general, the accuracy of the underlying models for the pressure-strain and dissipation rate etc. can be questionable. A more sound approach should be to develop underlying models that are as accurate as possible for a large number of flows and to investigate the corresponding shortcomings with respect to variations of the model parameters. In this way the deficits of the fundamental model constituents can, hopefully, be weighed against each other when the final tuning of the model is performed. The differential Reynolds stress model (DRSM) proposed by Sjögren and Johansson [1] (SJ-DRSM) is a relevant example of this. In the development of the SJ-DRSM, nonlinear modelling was used in order to force the underlying models to separately satisfy realizability. For the higher order models this left, depending on the order, a number of free parameters that were calibrated by studying the total closure predictions for fully developed rotating channel flow.

Previous related studies include the classical investigation by So et al. [2]. In their study, a large number of different RANS-closures are tested for nonrotating channel flow and comparisons are made with DNS-data from Kim et al. [3]. In a study of rotating Couette flow, Pettersson and Andersson [4] conducted RANS-computations by using a cross-stream two-dimensional computational domain. Jakirlić and K. Hanjalić [5] performed a priori tests in their work which involved the development of a new approach to modelling near-wall turbulence and stress dissipation rate. Kaltenbach [6] made a priori tests of wall models for separated flows.

Fully developed rotating channel flow is a test case that provides challenging modelling difficulties. This flow case has been studied numerically by, for instance, Kristoffersen and Andersson [7], Piomelli and Liu [8], Lamballais et al. [9] and Alvelius [10]. Experimental studies have been performed by, e.g., Johnston et al. [11]. The spanwise system rotation, of this case, gives rise to a Coriolis force that divides the channel into two areas, one stable and one unstable region located in the suction and pressure sides of the channel, respectively. For intermediate rotation numbers this implies that the increased mixing on the unstable side leads to higher turbulence levels while the response on the stable side of the channel is the opposite. For very high rotation numbers the increased rotation has an overall damping effect on the turbulence.

The aim of the present study is to perform a priori investigations of pressure-strain and dissipation rate models for fully developed turbulent channel with and without rotation and thereby illustrate the modelling difficulties when a wide range of rotation numbers are considered. Furthermore, ideal behaviour of model parameters with respect to least-squares optimizations is also considered which clearly illustrates the modelling difficulties associated with a wide range of rotation numbers.

The pressure-strain rate models tested are the SJ-model proposed by Sjögren and Johansson [1], the SSG-model by Speziale et al. [12] and the model corresponding to the curvature corrected version of the explicit algebraic Reynolds stress model (EARSM) by Wallin and Johansson [13] (CC-WJ), see Wallin and Johansson [14]. Three models for the dissipation rate tensors are considered, the SJ-model, the standard isotropic model and simplest possible extension of the isotropic model including a linear contribution of the Reynolds stress anisotropy tensor. Of primary interest is the response of the models to the gradually increased rotation. We are of the opinion that the set of chosen models reflects the range of formulations available today. While the SSG-model is widely used, the CC-WJ model is quasilinear and is hence suitable for EARSM development. The SJ-model is, on the other hand, a nonlinear model derived by imposing realizability on each of the terms.

2. Governing equations

The equations governing rotating channel flow are given by the Navier–Stokes equations, preferably formulated in a rotating frame of reference. These and the continuity condition are given by

$$\frac{\partial \tilde{u}_i}{\partial t} + \tilde{u}_j \frac{\partial \tilde{u}_i}{\partial x_j} = -\frac{1}{\rho}\frac{\partial \tilde{p}^*}{\partial x_i} + \nu \frac{\partial^2 \tilde{u}_i}{\partial x_j \partial x_j} + 2\epsilon_{ijk}\tilde{u}_j \omega_k, \tag{1}$$

$$\frac{\partial \tilde{u}_i}{\partial x_i} = 0, \tag{2}$$

where $\tilde{u}_i$ is the ith component of the instantaneous velocity and $\tilde{p}^* = \tilde{p} - \frac{\rho}{2}(\epsilon_{klm}\omega_l x_m \epsilon_{kpq}\omega_p x_q)$ (assuming that the origin is located on the rotation axis) is the reduced pressure in which the centrifugal acceleration has been absorbed. ω_i is the ith component of the system rotation rate vector and ω is the absolute value. For channel flow with spanwise rotation this implies that the components of the rotation rate vector are given by $\omega_i = \omega\delta_{i3}$, in a coordinate system that has the streamwise, wall-normal and spanwise directions numbered first, second and third, respectively. The components of the velocity field are also denoted u, v and w in the respective directions. The instantaneous velocity and pressure fields can be decomposed into mean and fluctuating parts as $\tilde{u}_i = U_i + u_i$ and $\tilde{p} = P + p$, where $U_i = \overline{\tilde{u}_i}$ and $P = \overline{\tilde{p}}$ and where a bar means an averaged quantity. For fully developed rotating turbulent channel flow the only nonzero mean velocity component is that in the streamwise direction, U_1, here simply denoted U. Therefore, the equation governing the mean flow is obtained by averaging (1) and is given by

$$\frac{\partial U}{\partial t} = -\frac{1}{\rho}\frac{\partial P}{\partial x_i} + \frac{\partial}{\partial y}\left(\nu\frac{\partial U}{\partial y} - \overline{uv}\right). \tag{3}$$

Note that there is hence no explicit dependence on the system rotation rate in the mean flow equation. The influence of the system rotation on the mean flow enters solely through the Reynolds shear stress, $\overline{uv}$. In order to be able to solve the equation governing the mean flow, $\overline{uv}$ which so far is an unknown, must be modelled using some sort of RANS-turbulence model. Studying this particular task is, however, not the purpose of the present investigation and will therefore not be further discussed. Of interest, on the other hand, are the modelling assumptions necessary for the full transport equation of the Reynolds stresses. This equation, can in schematic form be written

$$\frac{D\overline{u_i u_j}}{Dt} = \mathcal{P}_{ij} - \varepsilon_{ij} + \Pi_{ij} - \frac{\partial}{\partial x_m}\left(J_{ijm} - \nu\frac{\partial \overline{u_i u_j}}{\partial x_m}\right) + C_{ij}, \tag{4}$$

where $D/Dt = \partial/\partial t + U_k\partial/\partial x_k$ is the advection due to the mean flow. In the case of fully developed channel flow the left-hand side of (4) vanishes in a rotating frame of reference. The three first terms in (4) represent production, dissipation and pressure-strain rates. The last term represents volume forces while the remaining terms are associated with diffusion, turbulent and molecular. These terms are defined as

$$\mathcal{P}_{ij} = -\overline{u_i u_m}\frac{\partial U_j}{\partial x_m} - \overline{u_j u_m}\frac{\partial U_i}{\partial x_m}, \tag{5}$$

$$\varepsilon_{ij} = 2\nu\overline{u_{i,m}u_{j,m}}, \tag{6}$$

$$\Pi_{ij} = \frac{2}{\rho}\overline{p s_{ij}}, \tag{7}$$

$$J_{ijm} = \overline{u_i u_j u_m} + \frac{1}{\rho}(\overline{u_j p}\delta_{im} + \overline{u_i p}\delta_{jm}), \tag{8}$$

$$C_{ij} = \overline{u_i f_j} + \overline{u_j f_i}. \tag{9}$$

For system rotation, the volume force is given by $f_i = -2\varepsilon_{ilm}\omega_l u_m$. $_{,m}$ denotes the derivative with respect to the mth spatial coordinate. The production can be expressed exactly in terms of the quantities that are being solved for while the dissipation, pressure-strain and diffusion rate tensors have to be modelled. The pressure-strain rate tensor is often split into three parts, the rapid, slow and Stokes parts. This split is due to the characteristics of the formal solution of the Poisson equation for the fluctuating pressure which can be written as (see Hallbäck et al. [15])

$$-\frac{1}{\rho}p_{,kk} = \underbrace{2U_{i,j}u_{j,i}}_{-\frac{1}{\rho}p^{(r)}_{,kk}} + \underbrace{u_{i,j}u_{j,i} - \overline{u_{i,j}u_{j,i}}}_{-\frac{1}{\rho}p^{(s)}_{,kk}} \tag{10}$$

with the wall boundary condition

$$\frac{1}{\rho}p_{,2} = \nu u_{2,22}, \tag{11}$$

where x_2 is the wall-normal direction. The rapid and slow parts of the fluctuating pressure are denoted $p^{(r)}$ and $p^{(s)}$ in (10), respectively, and are subject to homogeneous Neumann wall boundary conditions. The Stokes pressure, on the other hand, is governed by a (homogeneous) Laplace equation with an inhomogeneity of the Neumann wall boundary

condition that is equal to the right-hand side of (11). The rapid part involves the mean velocity gradient and hence directly (rapidly) responds to a change in the mean flow. The slow and Stokes parts, on the other hand, are only dependent on the fluctuating velocities and hence their response to changes in the mean flow is not as direct. The Stokes term, is not included in the present investigation. The most important reason for this is that in comparison to the other parts, the Stokes term is very small. Furthermore, in many models the Stokes part is not given any special attention. The evaluation of the DNS-data has been done in accordance with (10) and (11).

It should be pointed out that (5) is the production formulated in the rotating frame of reference. The Coriolis term, as given in (9), results from the transformation from an inertial to a rotating frame of reference and is composed of two equal parts, one from the transformation of the production and one from the transformation of the advection. If instead the production is formulated in an inertial system, half of the Coriolis term C_{ij} would be accounted for by the production. The "remaining half" of the Coriolis term, which still appears in the governing equations, would emanate from the advection.

The formulation above, (5) and (9), is a natural result of the form of the equation governing the instantaneous velocity field (1). In RANS-modelling where the production usually is expressed in terms of symmetric and antisymmetric tensors formed from the mean velocity gradients, the contribution from system rotation is naturally included in the transformation from the inertial to the rotating system, see for instance Wallin and Johansson [13].

A rotation number based on the (spanwise) system rotation rate can be defined as

$$Ro = \frac{2\delta\omega}{U_b}. \tag{12}$$

$U_b = \frac{1}{2\delta}\int_{-\delta}^{+\delta} U(y)\,\mathrm{d}y$ is the mean bulk flow and δ is the channel half-width. This relates the velocity scale induced by the system rotation to the mean bulk flow. Since U_b is indirectly influenced by the system rotation rate through the behaviour of the Reynolds shear stress, the rotation number is not directly proportional to the system rotation rate, ω. This applies under the assumption that the pressure gradient is kept constant for the different rotation rates. Reynolds numbers of interest can be based on either the mean bulk velocity, U_b or the wall-shear velocity, $u_\tau = \sqrt{\nu\,\mathrm{d}U/\mathrm{d}y|_{\mathrm{wall}}}$ as

$$Re_b = \frac{\delta U_b}{\nu}, \tag{13}$$

$$Re_\tau = \frac{\delta u_\tau}{\nu}. \tag{14}$$

In rotating channel flow the wall-shear velocities of the stable and unstable side are denoted u_τ^s and u_τ^u, respectively. They relate to the total wall shear velocity through, $u_\tau = \sqrt{u_\tau^{s2}/2 + u_\tau^{u2}/2}$, which is unaffected by the system rotation since the pressure gradient is constant and the force balance must be fulfilled.

2.1. Models

In the present study we shall investigate a number of models used for the pressure-strain and dissipation rates of the Reynolds stresses. Especially the modelling of the pressure-strain will be in focus and three models will be investigated; the quasi-linear model used by for instance Wallin and Johansson [14] denoted CC-WJ, the SSG-model proposed by Speziale et al. [12] and the strongly nonlinear model by Sjögren and Johansson [1].

The model by Sjögren and Johansson [1] (SJ-model) is algebraically somewhat lengthy and is therefore presented in Appendix A. It should be pointed out that this model has been tested with and without the nonlinear (in the mean velocity gradients) extensions given by (48) and (49) in Appendix A. The version including these extensions is denoted SJN while the version without will be denoted SJ.

The CC-WJ and the SSG models are much more compact and can be written using the same tensorial expression which reads

$$\begin{aligned}\frac{\boldsymbol{\Pi}}{\varepsilon} - \mathbf{e} = &-\frac{1}{2}\left(C_1^0 + C_1^1\frac{\mathcal{P}}{\varepsilon}\right)\mathbf{a} + \left(C_2 - \frac{C_2^*}{2}\sqrt{\{\mathbf{a}^2\}}\right)\tau\mathbf{S} + \frac{C_3}{2}\tau\left(\mathbf{aS} + \mathbf{Sa} - \frac{2}{3}\{\mathbf{aS}\}\mathbf{I}\right)\\ &- \frac{C_4}{2}\tau(\mathbf{a}\boldsymbol{\Omega} - \boldsymbol{\Omega}\mathbf{a}) + \frac{C_5}{4}\left(\mathbf{a}^2 - \frac{1}{3}\{\mathbf{a}^2\}\mathbf{I}\right)\end{aligned} \tag{15}$$

Table 1
The values of the C coefficients for different pressure-strain models

	C_1^0	C_1^1	C_2	C_2^*	C_3	C_4	C_5
Original LRR	3.0	0	0.8	0	1.75	1.31	0
CC-WJ	4.6	1.24	0.47	0	2	0.56	0
SSG	3.4	1.8	0.8	1.30	1.25	0.40	4.2
IP	3.6	0	0.8	0	1.2	1.2	0

in which a boldface matrix notation has been used. $\{\cdot\}$ denotes the trace and $\mathbf{I}$ is the identity. The components of the dissipation rate and Reynolds stress anisotropy tensors, $\mathbf{e}$ and $\mathbf{a}$, are given by $e_{ij} = \varepsilon_{ij}/\varepsilon - 2\delta_{ij}/3$ and $a_{ij} = \overline{u_i u_j}/K - 2\delta_{ij}/3$, respectively. $K = \overline{u_i u_i}/2$ is the turbulence kinetic energy and $\tau = K/\varepsilon$ is the turbulence timescale. The mean strain and rotation rate tensors have components given by

$$S_{ij} = \frac{1}{2}\left(\frac{\partial U_i}{\partial x_j} + \frac{\partial U_j}{\partial x_i}\right), \qquad \Omega_{ij} = \frac{1}{2}\left(\frac{\partial U_i}{\partial x_j} - \frac{\partial U_j}{\partial x_i}\right) - \epsilon_{ijk}\omega_k, \tag{16}$$

where ω_k is the k-th component of the system rotation rate vector. For this particular study in which spanwise rotation is considered, $\omega_k = \omega\delta_{3k}$. It should be pointed out that the absolute rotation rate tensor is given in (16). The occurrence of the system rotation rate, ω, is a direct result of transforming the rotation rate tensor from a inertial to a rotating frame of reference.

The coefficients corresponding to the different proposed models are given in Table 1. The CC-WJ coefficients corresponds to the curvature corrected EARSM developed by Wallin and Johansson [14]. Classical linear models, such as the LRR-model excluding the wall term, Launder et al. [16], or the simplified so called isotropization of production (IP) model, see Naot et al. [17], may be written in this form as well. The coefficients for these models are also given in Table 1.

The above modelling approach (15) is mathematically (but not physically) indistinguishable from modelling the total pressure-strain with the right-hand side of (15) and the dissipation with an isotropic model as

$$\boldsymbol{\varepsilon} = \frac{2}{3}\varepsilon\mathbf{I}, \tag{17}$$

where $\varepsilon = \varepsilon_{ii}/2$. This is in fact the underlying assumption in the a priori test of the present investigation. It is necessary to make such a choice in order to be able to distinguish between the modelling of the slow pressure-strain and dissipation rate tensors. The dissipation rate model by Sjögren and Johansson [1] is presented in Appendix A and will be tested and compared with (17).

In the present study, the pressure-strain is divided into rapid and slow parts. The terms of (15) that in any form include mean velocity gradients are said to belong to the rapid part of the pressure-strain rate model. These terms have coefficients C_1^1, C_2, C_2^*, C_3 and C_4. Speziale et al. [12] opposed the splitting of their model into rapid and slow parts. However, the fact still remains that a certain (the rapid) part of the model responds rapidly to changes in the mean flow.

3. A priori tests

All flow data used in the present investigation were obtained through the direct numerical simulations by Alvelius [10]. Alvelius [10] used the pseudo-spectral code by Lundblad et al. [18], with Fourier series in the periodic streamwise and spanwise directions and Chebychev polynomials in the wall-normal direction. Data from simulations at $Re_\tau = u_\tau\delta/\nu = 180$ and 360 have been used. The rotation numbers considered are $Ro = 2\delta\omega_3/U_b = 0$ and 0.20 for $Re_\tau = 360$ and $Ro = 0.43$ and 0.77 for $Re_\tau = 180$.

3.1. Balance of the Reynolds stress equation

In what follows the production is formulated relative to the rotating reference frame, as given by (5). Correspondingly, the Coriolis term is evaluated according to (9). For nonrotating channel flow, the production contributes only to the $\overline{uu}$- and $\overline{vv}$-components. For both $\overline{uu}$ and $\overline{uv}$ the pressure-strain rate tensor has the opposite sign as compared to the production and therefore redistributes energy to the $\overline{vv}$- and $\overline{ww}$-components for which the respective pressure-strain rate components are positive.

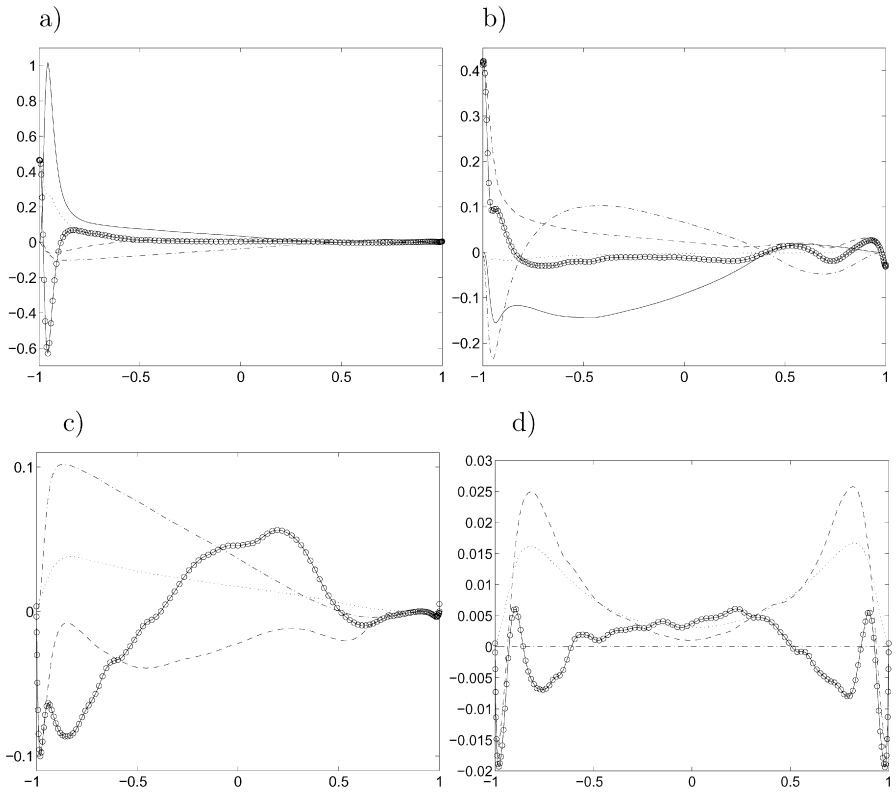

Fig. 1. Budgets for $Re_\tau = 180$ at $Ro = 0.43$ for (a) $\overline{uu}$-component, (b) $\overline{uv}$-component and (c) $\overline{vv}$-component. (d) $\overline{vv}$-component for $Ro = 0.0$. $\mathcal{P}_{ij}^+$ $(-)$, Π_{ij}^+ $(--)$, ε_{ij}^+ $(\cdots)$, $\mathcal{C}_{ij}^+$ $(-\cdot)$ and $\mathcal{D}_{ij}^+$ $(-\circ)$.

For an intermediate rotation number of $Ro = 0.43$, the terms of major importance for the $\overline{uu}$-component are the production and Coriolis terms, see Fig. 1(a). The pressure-strain and diffusion terms gain influence closer to the wall on the unstable side. The major contributor to the $\overline{vv}$-component is the Coriolis term while the pressure-strain rate tensor drains this component of energy which is the opposite of what happens for the nonrotating case, see Figs. 1(c) and 1(d). The $\overline{ww}$-component is rather passive in this sense and is given energy only by the pressure-strain rate tensor. It is also unaffected by the Coriolis term. For the $\overline{uv}$-component, the Coriolis, production and pressure-strain rate terms are dominating in the center of the channel. The Coriolis term changes sign twice and has, as the pressure-strain rate term, a suppressing effect in the center of the channel, see Fig. 1(b). Closer to the walls, the diffusion gains influence. For the highest rotation number, $Ro = 0.77$, the relation between the different terms remain the same more or less. The region with the dominating magnitudes are, however, shifted towards the wall in the unstable side.

Some concluding remarks can be made regarding the balance of the Reynolds stress transport equation. The turbulence diffusion of the different components has a rather complicated behaviour but has a tendency to correlate with the second derivative of the respective component which makes gradient-based modelling feasible. From a modelling point of view, the biggest challenge should be to capture the behaviour of the pressure-strain rate tensor. Not only because its behaviour is complex, e.g. the change of sign for the $\overline{vv}$-component, but also due to the fact that the magnitude is relatively large in comparison to that of the other modelled terms.

3.2. Pressure-strain rate tensor

The a priori evaluations in the present investigation are performed by using mean flow, Reynolds stress and dissipation rate statistics from DNS. The actual evaluation is performed by inserting the DNS data in the expression for the model to be evaluated. The results of this exercise for the two versions (SJ and SJN) of the SJ-model, Sjögren and

Johansson [1], the SSG and CC-WJ models are shown in Figs. 2–4. SJN and SJ make very similar predictions for the cases tested here. Therefore, SJN is not discussed separately.

Figs. 2–4 show the components of the rapid ($\Pi_{ij}^{(r)}$) and slow ($\Pi_{ij}^{(s)}$) pressure-strain rate models for $Re_\tau = 360$ and $Ro = 0.0$ (Fig. 2), $Re_\tau = 360$ and $Ro = 0.20$ (Fig. 3) and $Re_\tau = 180$ and $Ro = 0.77$ (Fig. 4). The components of the exact rapid and slow parts of pressure-strain rate tensor evaluated from the DNS are shown for comparison in the respective plot.

In the center of the channel the different model predictions are on par with the DNS for the nonrotating case. Closer to the wall both the CC-WJ and the SSG-model give rapid pressure-strain rate tensor components of excessive

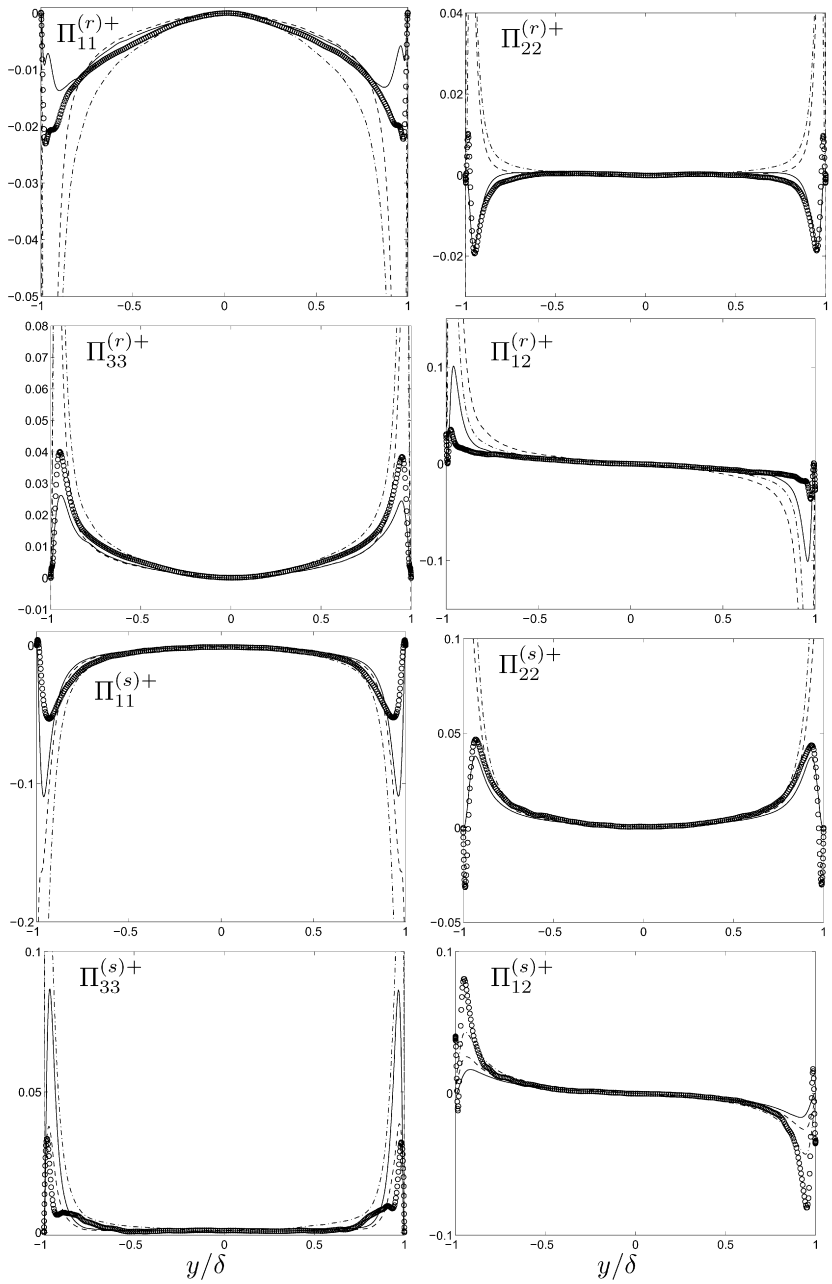

Fig. 2. Rapid and slow pressure-strain normalized with wall units for $Re_\tau = 360$ and $Ro = 0.0$. DNS (∘), SJ (−), SSG (−−), CC-WJ (−·) and SJN (···).

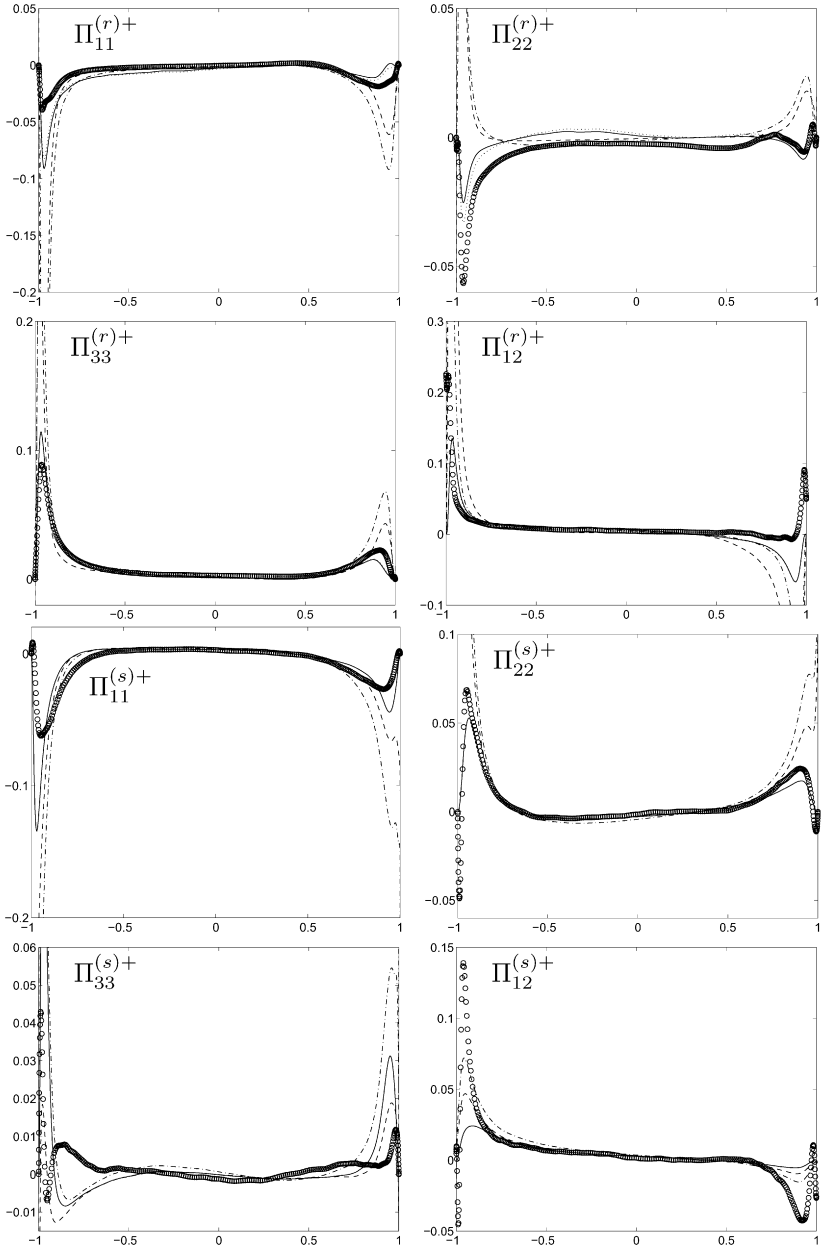

Fig. 3. Rapid and slow pressure-strain normalized with wall units for $Re_\tau = 360$ and $Ro = 0.20$. DNS (○), SJ (−), SSG (−−), CC-WJ (−·) and SJN (···).

magnitudes. The need for some sort of damping is obvious. This is also the case for the $\overline{uu}$- and $\overline{vv}$-components of the slow pressure-strain. The SSG-model does however, make good predictions of the $\overline{ww}$-component of the slow pressure strain. All models underestimate the magnitude of the $\overline{uv}$-component of the slow pressure-strain rate. The SJ-DRSM shows a much more controlled behaviour close to the wall. The $\overline{vv}$-component is in excellent agreement for the slow and rapid parts, respectively. This is the component for which the other two models show the worst deficits in their prediction of a positive $\overline{vv}$-rapid-pressure-strain-rate component. For the remaining components, the SJ-DRSM is in significantly better agreement with the DNS than the other models but gives, nevertheless, substantial deviations for the separate parts of the pressure strain. Interesting though is that the error in the respective parts tend to cancel each other making the predictions of the total pressure-strain rate model relatively accurate. While the prediction of the

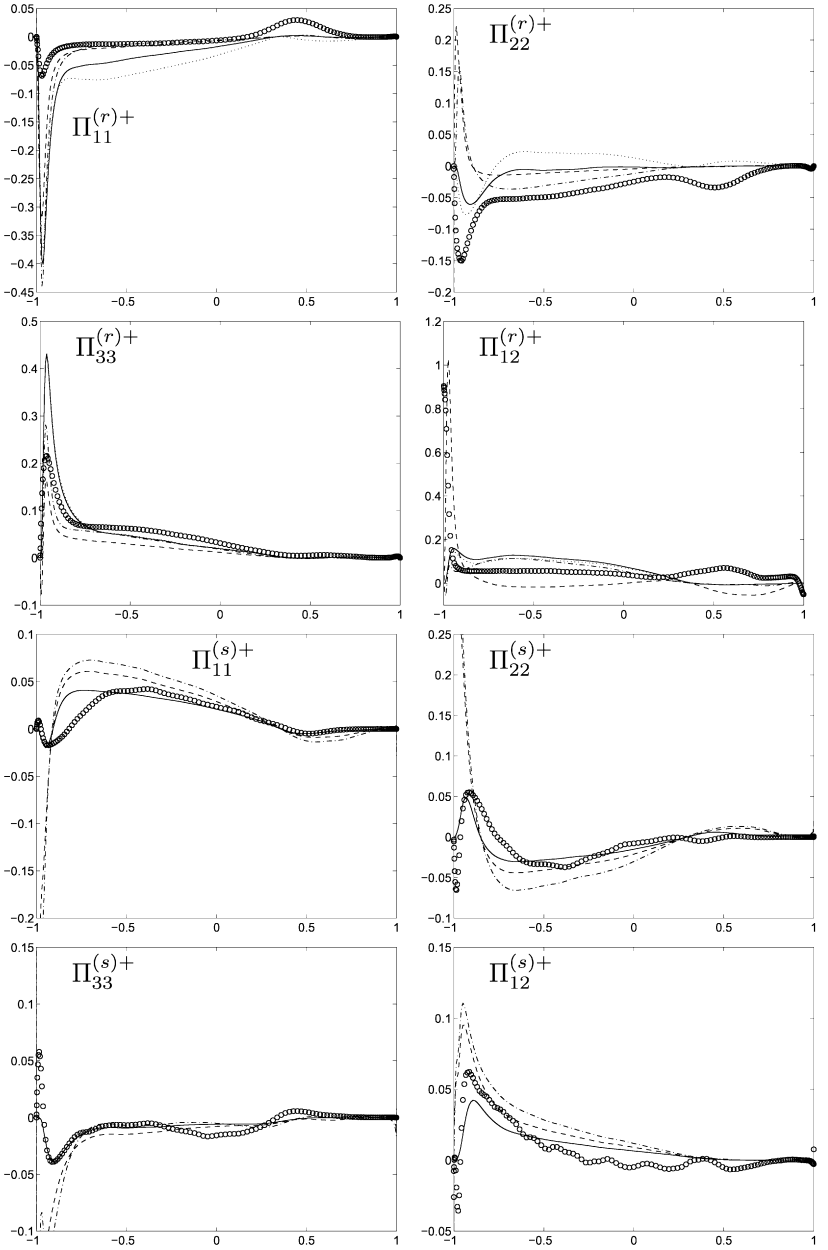

Fig. 4. Rapid and slow pressure-strain normalized with wall units for $Re_\tau = 180$ and $Ro = 0.77$. DNS (∘), SJ (−), SSG (−−), CC-WJ (−·) and SJN (···).

$\overline{vv}$-component of the total pressure-strain rate of the SJ-DRSM is rather accurate, the corresponding $\overline{uu}$-component is slightly under predicted which due to tracelessness implies an over prediction of the $\overline{ww}$-component.

When system rotation is applied, the Coriolis effects lead to decreased magnitudes on the stable side compared to the unstable side for both simulations and models and in many cases the magnitudes are lower than for the nonrotating flow. Near the wall on the stable side of the channel, all modelled pressure-strain rate components are comparable to those of the DNS. The lack of near-wall treatment for the CC-WJ and the SSG-model on the unstable side are still, however, obvious, the magnitudes are over predicted and nonzero values on the wall of the $\overline{uu}$- and $\overline{vv}$-components of the slow pressure-strain rate are obtained. Furthermore, the sign of the $\overline{vv}$-component is still wrong for the rapid pressure-strain rate for the CC-WJ and SSG-models. The SJ-DRSM, once more, makes the most accurate predictions.

It should be noted that the $\overline{uv}$-components of the total pressure-strain rate is nonzero at the wall on both sides of the channel. This is something that none of the tested models are able to capture which implies that differences in the wall-shear velocity of the stable and unstable side between DNS and RANS-computations using any of the investigated models, should be expected.

For the highest rotation number, $Ro = 0.77$, in the present study, the comparisons are based on simulations for $Re_\tau = 180$. On the stable side of the channel, where the turbulence has been suppressed severely and the magnitudes of the DNS are relatively small, all models have difficulties capturing the correct behaviour. The model behaviour in the center of the channel clearly deviates more from the DNS than for the lower rotation numbers. The problems are most significant close to the wall on the unstable side where all models are far off in their predictions of the $\overline{uu}$-component for the both the slow and rapid pressure-strain rates. The CC-WJ and SSG-model also miss out on the $\overline{vv}$-component for the same quantities and do, in addition, give nonzero values on the wall of the slow part. The CC-WJ does, however, provide the most accurate predictions of the $\overline{uv}$-component of the total pressure-strain rate tensor.

3.3. Dissipation rate tensor

Three different models for the dissipation rate tensor are investigated, the model proposed by Sjögren and Johansson [1], the isotropic model (17) and the isotropic model including a term proportional to the Reynolds stress anisotropy tensor which can be written

$$\boldsymbol{\varepsilon} = \frac{2}{3}\varepsilon \mathbf{I} + c_p \varepsilon \mathbf{a}. \tag{18}$$

In the present study two values of c_p have been used, 0.5 and 1. The particular choice of $c_p = 1$ gives $\varepsilon_{22} = 0$ at the wall in accordance with the DNS-data and by analyzing (6). With respect to this, the $c_p = 0.5$ model represents an intermediate form (consistent with rapid distortion theory), included to demonstrate the trend of increasing c_p. It can be pointed out that the part of the CC-WJ model with $C_1^0 = 4.6$ corresponds to a Rotta model (Rotta [19]) with $\boldsymbol{\Pi}^{(s)} = -1.8\varepsilon\mathbf{a}$ together with a linear dissipation rate anisotropy model with $c_p = 0.5$. This is realized from the general expression for the total pressure-strain and dissipation rate anisotropy tensor model (15).

The components of the modelled dissipation rate tensors are plotted for $Re_\tau = 360$ ($Ro = 0.0$ and $Ro = 0.20$) in Fig. 5 and $Re_\tau = 180$ for $Ro = 0.77$ in Fig. 6. The SJ-model gives diagonal components in very good agreement with the DNS-data for all rotation numbers. The isotropic model misses out severely for many components and, e.g., gives a nonzero ε_{22} at the wall. It is interesting to see that the model corresponding to (18) (labelled as "$c_p = 0.5$" and "$c_p = 1$" in the captions of Figs. 5 and 6) gives significantly better predictions than the isotropic model. The model corresponding to $c_p = 1$ is close to, and can for some components and rotation numbers be hard to distinguish from the SJ-model. For increased rotation numbers, the different models give increasingly similar predictions. The model given by (18) for $c_p = 0.5$ has the best overall performance regarding ε_{12}. This component of the dissipation rate tensor is, however, of little importance in the balance of the transport equation of the corresponding Reynolds stress, see Fig. 1(b). It should be noted that the isotropic model, naturally, gives $\varepsilon_{12} = 0$ for all rotations.

4. Ideal behaviour of model parameters

The linear form of the pressure-strain rate models is indeed the most common kind of model and many different formulations have been proposed. Differences can consist in, for instance, parameter calibration and near-wall treatments. No new pressure-strain rate model is proposed in the present work. Instead, we will investigate the ideal behaviour of the model coefficients by optimizing the coefficients for a given set of model tensors. This is done locally point-by-point and will result in, from a least-squares point of view, optimal distributions of the model coefficients. The derivation procedure is similar to the framework discussed by for instance, Jongen and Gatski [20], Gatski and Jongen [21] and Grundestam et al. [22].

For fully developed turbulent channel flow, with or without system rotation, the pressure-strain rate tensor, the rapid as well as the slow, has three independent components due to being traceless and having zero 31- and 32-components. It is therefore possible to exactly represent the pressure-strain rate tensor in terms of three basis tensors which fulfill the necessary conditions. This assumes that dependencies of the representation coefficients on invariants involving the

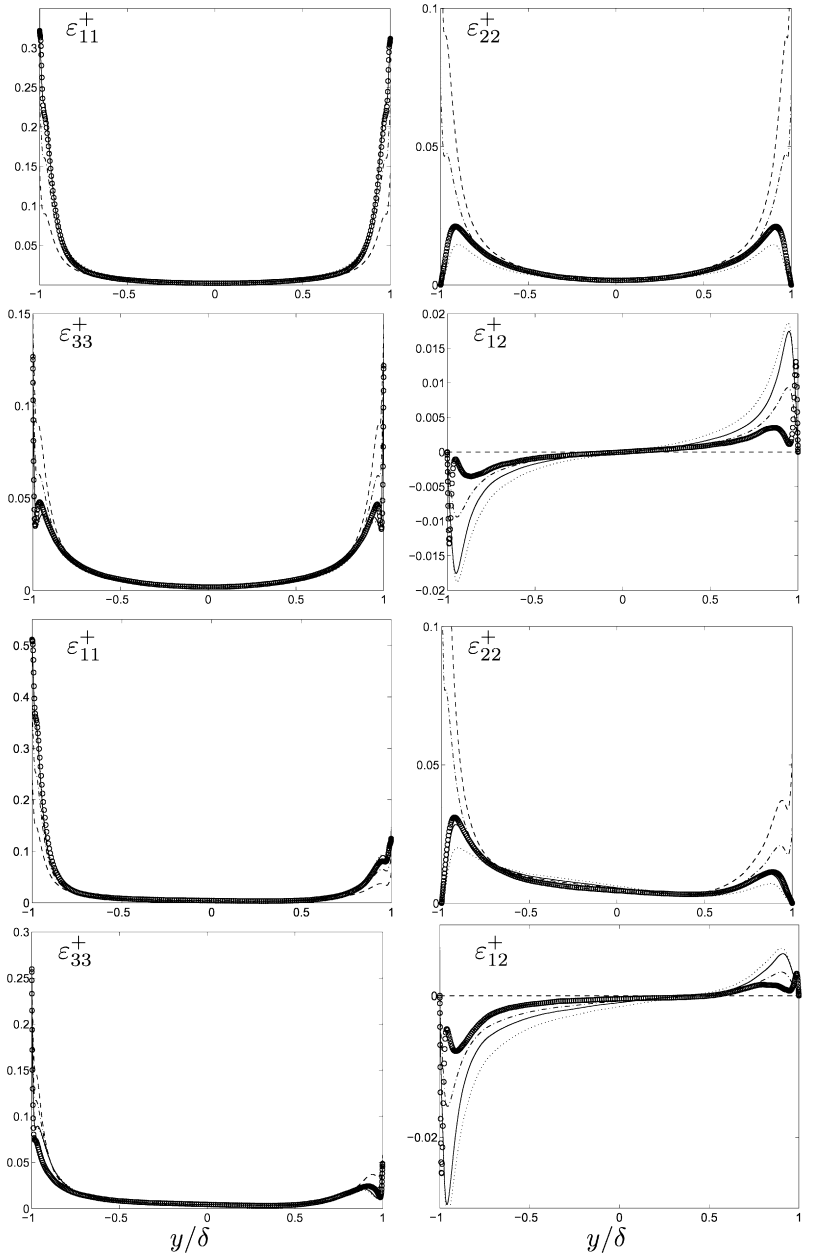

Fig. 5. Dissipation rate tensor for $Re_\tau = 360$ and $Ro = 0.0$ (top) and $Ro = 0.20$ (bottom). DNS (∘), SJ (−), isotropic (−−), $c_p = 0.5$ (−·) and $c_p = 1$ (···).

pressure-strain rate tensor itself are allowed. These basis tensors must be independent, traceless and have the same zero components as the pressure-strain rate tensor. Three tensors that can be used for this are given by

$$\mathbf{B}^{(2)} = \mathbf{S},$$
$$\mathbf{B}^{(3)} = \mathbf{aS} + \mathbf{Sa} - \frac{2}{3}\{\mathbf{aS}\}\mathbf{I},$$
$$\mathbf{B}^{(4)} = \mathbf{a}\boldsymbol{\Omega} - \boldsymbol{\Omega}\mathbf{a}, \tag{19}$$

where $\mathbf{S}$ and $\boldsymbol{\Omega}$ have been nondimensionalized with τ and $\boldsymbol{\Omega}$ is the absolute rotation rate tensor defined in (16). These are especially suitable since they are all included in the general expression for the pressure-strain rate model (15).

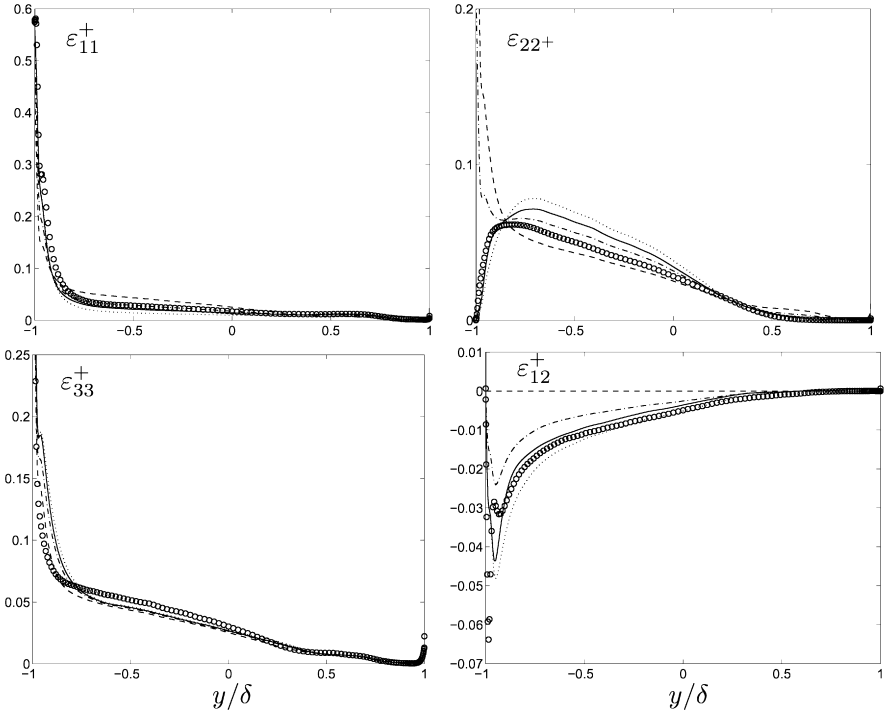

Fig. 6. Dissipation rate tensor for $Re_\tau = 180$ and $Ro = 0.77$. DNS (∘), SJ (−), isotropic (−−), $c_p = 0.5$ (−·) and $c_p = 1$ (···).

While both the rapid and slow parts can be represented with the tensors (19), representing the slow pressure-strain does not make sense from a physical point of view since its formal expression does not involve any explicit dependence on the mean velocity or its gradients. Therefore, the tensors (19) will be used only for studying the ideal behaviour of the coefficients of a linear model for the rapid pressure-strain rate tensor.

The corresponding representation coefficients for the rapid pressure-strain can be obtained by minimizing the error between $\boldsymbol{\Pi}^{(r)}$ itself and its representation given by

$$\tilde{\boldsymbol{\Pi}}^{(r)} = \varepsilon\left(C_2\mathbf{B}^{(2)} + \frac{C_3}{2}\mathbf{B}^{(3)} - \frac{C_4}{2}\mathbf{B}^{(4)}\right) \tag{20}$$

in a least square sense. Multiplication by ε is needed in order to give $\tilde{\boldsymbol{\Pi}}^{(r)}$ the right dimension since $\mathbf{S}$ and $\boldsymbol{\Omega}$ have been nondimensionalized, as pointed out above. The form of the coefficients has been chosen to be consistent with the general expression (15). The derivation of the algebraic form of the C-parameters is performed by evaluating the trace of the square of the error, $\mathbf{E} = \boldsymbol{\Pi}^{(r)} - \tilde{\boldsymbol{\Pi}}^{(r)}$, differentiating with respect to each of the representation coefficients and setting the corresponding expressions equal to zero according to

$$\frac{\partial\{\mathbf{E}^2\}}{\partial C_k} = 0, \quad k = 2, 3, 4. \tag{21}$$

By studying, e.g., Gatski and Jongen [21] and working out the algebra one can deduce that (21) yields a system of linear equations for the representation coefficients that can be written as

$$\sum_{k=2}^{4} c_k\left\{\mathbf{B}^{(k)}\mathbf{B}^{(p)}\right\} = \left\{\boldsymbol{\Pi}^{(r)}\mathbf{B}^{(p)}\right\}, \quad j = 2, 3, 4, \tag{22}$$

where $c_2 = C_2$, $c_3 = C_3/2$ and $c_4 = -C_4/2$ have been introduced for simplicity. The full expressions for the c_k-coefficients are given in Appendix B.

The representation coefficients will be dependent on invariants involving the basis tensors, $\mathbf{B}^{(i)}$ and the rapid pressure-strain rate tensor, $\boldsymbol{\Pi}^{(r)}$, as given by the DNS. The derived representation (20) can for this reason not be

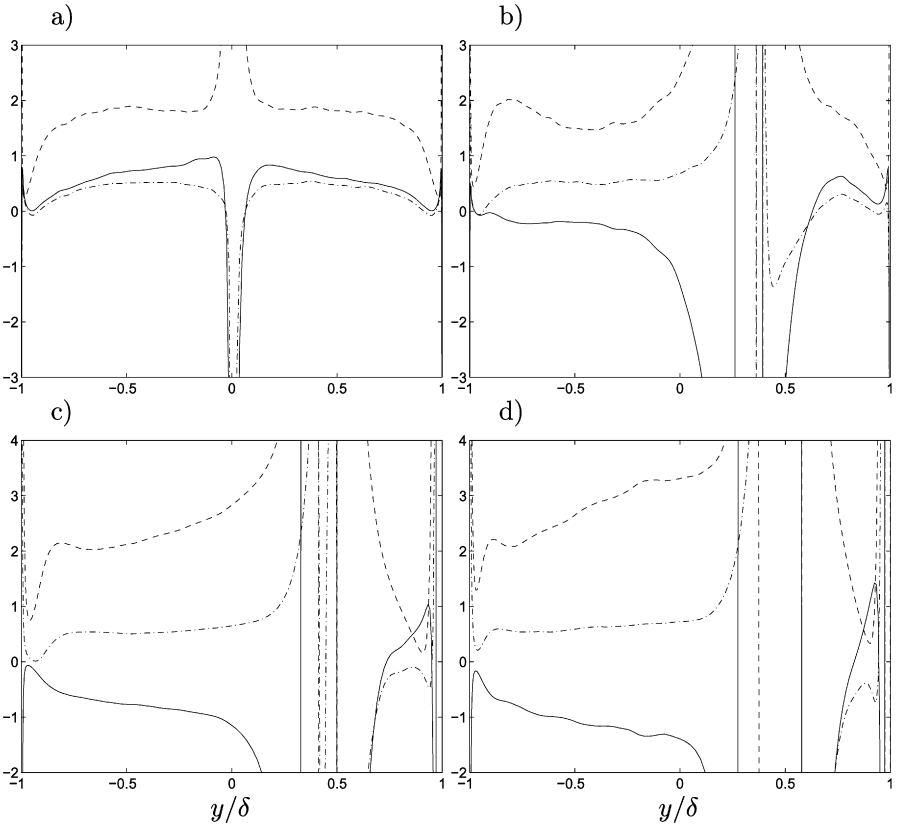

Fig. 7. Ideal behaviour of the coefficients of linear rapid pressure-strain rate model for channel flow at $Re_\tau = 360$ for (a) $Ro = 0.0$ and (b) $Ro = 0.20$ and at $Re_\tau = 180$ for (c) $Ro = 0.43$ and (d) $Ro = 0.77$. C_2 $(-\cdot)$, C_3 $(--)$ and C_4 $(-)$.

used as a RANS-model. The purpose is instead to study the model C-parameters which show how the parameters of a linear pressure-strain model would behave under the optimality assumptions above. For the particular case of rotating channel flow, for which the tensors (19) constitute a complete set, the representation (20) will be exact and exactly match the behaviour of the rapid pressure-strain rate tensor as given by the DNS. Hence, the behaviour of the C-parameters gives the ideal behaviour of the linear model parameters for this particular case. It should be pointed out that the optimality aspects of the representation (20) holds through the condition (21) also for flows where (19) does not constitute a complete basis.

The behaviour of the ideal C-parameters is shown in Fig. 7. The perhaps most striking feature of the ideal coefficients is their behaviour in the center of the channel or the corresponding region for the rotating cases. Their rapidly growing magnitudes are the result of singular-like behaviour due to small mean velocity gradients. Since the expressions for the C-parameters are given by rationals of polynomials of invariants involving the mean strain and rotation rate tensors, this can in some cases result in close-to-zero-over-zero behaviour. From a modelling point of view, however, this should not be a significant problem since the corresponding rapid pressure-strain rate components are small in this region. Of interest is instead the regions outside this area and close to the wall. The obvious need for damping close to the wall for the nonrotating case for the CC-WJ and SSG-model seen in Fig. 2 is reflected in the behaviour of the C-parameters seen in Fig. 7(a). When rotation is applied, C_2, is approximately constant in a region, on the unstable side of the channel, that grows with increasing rotation number. C_3 has a tendency to increase while C_4 decreases with increasing rotation and changes sign on the unstable side of the channel. In a region in the unstable side, the change of C_4 due to the increased rotation rate could be approximately described by a straight line going through the origin with a slope that decreases with increasing rotation number.

The outcome of this analysis can be directly compared to the original LRR-model, proposed by Launder et al. [16], with coefficients listed in Table 1. Based on nonrotating channel flow, the present study suggests the parameter values

$C_2 \sim 0.5$, $C_3 \sim 1.9$ and $C_4 \sim 0.7$. The discrepancies of the LRR-model are hence relatively large for the C_2- and C_4-coefficients for the nonrotating case. It should be pointed out that for the CC-WJ model, the agreement between the corresponding model parameters and those given in Fig. 7 is relatively good for the nonrotating case. However, due to a nonzero C_1^1, see (15), these two sets of parameters are not directly comparable. In order to be able to make direct comparisons with the CC-WJ model, the same tensorial form must be used for the representation as for the CC-WJ model. This can be obtained by including $\mathbf{a}$, corresponding to C_1^1 in (15), in the representation. For the present case with three independent components, however, the corresponding coefficients become singular. This can occur when the basis tensors become linearly dependent, see for instance Jongen and Gatski [20] and Grundestam et al. [22].

4.1. The slow pressure-strain and dissipation rate tensors

The procedure discussed above can also be applied to the slow pressure-strain and dissipation rate tensors. Neither one of these tensors have in their exact form an explicit dependence on the mean velocity. Therefore, the basis tensors should not have any dependence on the mean velocities or the corresponding gradients. In ordinary RANS-closures, where the Reynolds stress anisotropy (or just Reynolds stress) tensor is the only available tensor quantity suitable for the present modelling, one is restricted to the basis tensors

$$\begin{aligned} \mathbf{b}^{(1)} &= \mathbf{a}, \\ \mathbf{b}^{(2)} &= \mathbf{a}^2 - \frac{1}{3} II_{\mathbf{a}} \mathbf{I}. \end{aligned} \tag{23}$$

It should be realized that tensors including higher powers of $\mathbf{a}$ than two, can be reduced to a combination of (23) through the Cayley–Hamilton theorem. The corresponding representations for the slow pressure-strain and dissipation rate tensors read

$$\tilde{\boldsymbol{\Pi}}^{(s)} = \varepsilon\big(\eta_1 \mathbf{b}^{(1)} + \eta_2 \mathbf{b}^{(2)}\big), \tag{24}$$

$$\tilde{\boldsymbol{\varepsilon}} = \varepsilon\left(\beta_1 \mathbf{b}^{(1)} + \beta_2 \mathbf{b}^{(2)} + \frac{2}{3}\mathbf{I}\right). \tag{25}$$

Note that the basis tensors (23) are traceless while the dissipation rate tensor is not. Therefore, the term $2\mathbf{I}/3$ must be included in (25) in order to fulfill $\{\boldsymbol{\varepsilon}\} = 2\varepsilon$. (25) does in fact correspond to modelling the dissipation rate anisotropy tensor as $\tilde{\mathbf{e}} = \beta_1 \mathbf{b}^{(1)} + \beta_2 \mathbf{b}^{(2)}$. The representation coefficients are derived with the procedure discussed above and are subject to the optimality condition (21). The full expressions for these coefficients are given at the end of Appendix B.

For channel flow the obtained representations (24) and (25), based on the basis tensors (23), are incomplete but still, however, optimal in the least square sense described above. This implies that the evaluations of the representations will not exactly match the corresponding quantities computed from the DNS data, for the particular case of channel flow.

The representation coefficients of the dissipation rate tensor, β_1 and β_2, are shown in Fig. 8 for $Re_\tau = 360$ at $Ro = 0.0$ and 0.20. In addition, the coefficient, $\beta_1^{(s)}$, corresponding to the representation including only the linear part, $\mathbf{a}$, as basis tensor, is plotted. As can be seen, aside from the singular-like behaviour in the center of the channel, the most dramatic rate of change is close to the wall. When rotation is applied to the channel, β_1 and $\beta_1^{(s)}$ are approximately unchanged on the unstable side of the channel. Note that β_1 and $\beta_1^{(s)}$ are close to each other with and without rotation indicating that the quadratic term of (25) is of less importance. It should be noted that the corresponding quadratic parameter of the SJ-model is zero. $\beta_1^{(s)}$ is also evaluated to be close to one at the wall which is consistent with $\varepsilon_{22} = 0$ as discussed above regarding the dissipation rate model (18). Worth noting is also that β_2 is close to zero in the region $-0.3 \leqslant y/\delta \leqslant 0$ for $Ro = 0.20$. It should be pointed out that both (25) and the representation corresponding to $\beta_1^{(s)}$ are very close to the SJ-model when evaluated. The $\beta_1^{(s)}$-representation, however, gives a nonzero $\overline{vv}$-component on the wall and a small region close to the wall with negative dissipation.

The η-coefficients of the representation of the slow pressure-strain rate tensor are plotted in Fig. 9. As for the dissipation, the representation coefficient, $\eta_1^{(s)}$, for the representation using only the linear part, $\mathbf{a}$, is also plotted. The same type of observation can be made for this case as for the dissipation. Both η_1 and $\eta_1^{(s)}$ are relatively unaffected by the system rotation away from the wall on the unstable side of the channel. They also attain approximately the same

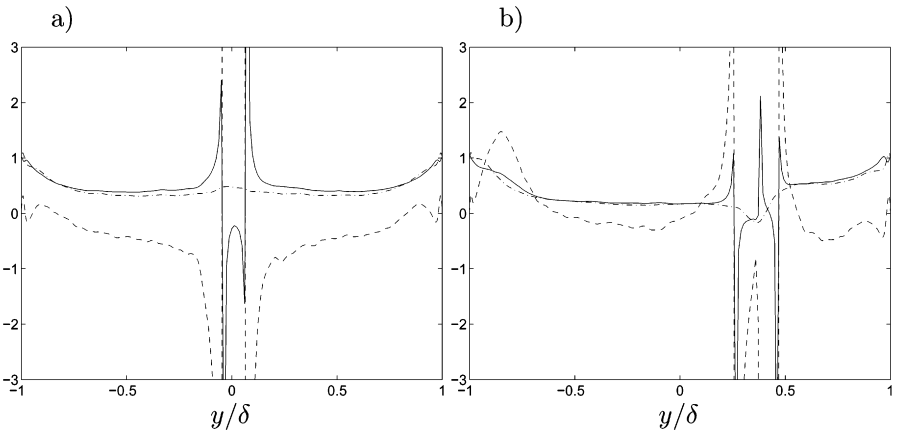

Fig. 8. Dissipation rate representation coefficients, β_1 and β_2, for $Re_\tau = 360$ at (a) $Ro = 0.0$ and (b) $Ro = 0.20$. β_1 (−), β_2 (−−) and $\beta_1^{(s)}$ (−·).

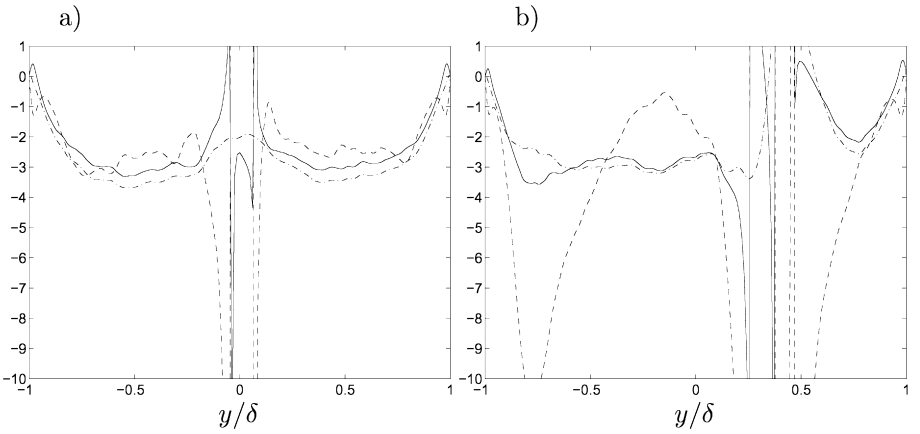

Fig. 9. Slow pressure-strain rate representation coefficients, η_1 and η_2, for $Re_\tau = 360$ at (a) $Ro = 0.0$ and (b) $Ro = 0.20$. η_1 (−), η_2 (−−) and $\eta_1^{(s)}$ (−·).

value indicating that also here the quadratic term is of less importance. For zero system rotation, η_2 behaves similar to η_1. System rotation apparently has a dramatic effect on η_2, see Fig. 9(b).

For the simplest possible linear modelling of the slow pressure-strain and dissipation rate tensors, the least-squares approach suggests that a constant coefficient for the slow pressure-strain rate should attain a value of $\eta_1^{(s)} \approx -3$ based on the region $-0.8 \leqslant y/\delta \leqslant -0.2$ for the nonrotating case. The parameter value for a linear dissipation rate model would be $\beta_1^{(s)} \approx 0.5$. This corresponds to the value obtained with rapid distortion theory (RDT), as discussed by Sjögren and Johansson [23]. In their paper, the Reynolds number dependence of $\eta_1^{(s)}$, based on experiments, is also studied. However, the plots in Figs. 5 and 6 indicate that for $\beta_1^{(s)} = 1$, the behaviour on the wall and in the near-wall region is radically improved, except for the 12-component, while the drawbacks in the center region of the channel are insignificant since the magnitude is small. Ultimately, this is a matter of choice and if some sort of near-wall treatment is to be included, the value corresponding to the center region should be considered. In all this suggests that a linear model for the added slow pressure-strain and dissipation rate tensors given by $\boldsymbol{\Pi}^{(s)} - \boldsymbol{\varepsilon} = -\varepsilon(C_1^0\mathbf{a}/2 + 2\mathbf{I}/3)$, should have a model parameter of $C_1^0 \sim 7$–8. This is considerably higher than for any of the models listed on Table 1. The CC-WJ model is closest to this with $C_1^0 = 4.6$ while the original LRR-model has a coefficient less than half of the least-squares value. It should be pointed out that a value corresponding to $\eta_1^{(s)} \to -3.6$ was suggested by Weinstock [24] in the limit of infinite turbulence Reynolds numbers, $Re_T = 4K^2/(\nu\varepsilon) \to \infty$. This is rather close to the value of $\eta_1^{(s)} \approx -3$ obtained with the least-squares analysis discussed above.

5. Discussion

The present investigation concerns a priori testing of different RANS turbulence models for the pressure-strain and dissipation rate tensors. The flow case considered is rotating and nonrotating channel flow and the flow data used were obtained in the DNS study by Alvelius [10]. Furthermore, least-squares based optimizations of the model coefficients are performed for a number of given base models. With the somewhat limited amount of DNS-data used there is non-negligible statistical uncertainty in the curves describing the ideal model coefficients. They are still smooth enough to yield interesting modelling conclusions.

The DNS-data used is based on averaging in the homogeneous stream- and spanwise directions and over a number of flow fields separated in time. This implies a dependence of the mean flow data on the wall-normal coordinate only. In rotating as well as curved channel flows, the existence of elongated Taylor–Görtler-vortice-like flow structures, roll cells, have been proven and discussed by numerous authors. These structures have an important influence on the mean flow through the enhanced mixing in the wall normal direction. Johnston et al. (1972) reported that the seen roll-cells had a very long time-scale, but that no truly steady structures were seen. The DNS by Kristoffersen and Andersson [7] showed that roll-cells persisted over the total sampling time of $5.6\delta/u_\tau$ for $Ro = 0.15$, but that the same structures were unsteady for all the other investigated rotation numbers. In a DNS study of rotating channel flow for a large span of rotation numbers performed in our group (Alvelius [10] and Grundestam et al. [25]), elongated streamwise structures were also found. However, no steady roll-cells were observed in the streamwise and time averaged field for sampling time spans of $\sim 82\delta/u_\tau$ ($\geqslant 1800\delta/U_b$, where U_b is the mean bulk velocity). In the spanwise and wall normal directions no scale separation between the roll cells and the rest of the turbulence have been observed and no well defined peak in the energy spectra has been reported. The structures are, thus, part of the turbulence, which is also the point of view for the present study.

Alternative approaches may be taken with other definitions of the averaging where the turbulence is partly resolved. Unsteady RANS, RANS-LES hybrid methods and also LES fall into this category. In a computational study by Pettersson and Andersson [4] using a RANS approach, these roll cells were captured in the averaged and resolved field by using a two-dimensional cross-stream computational domain assuming steady mean flow and homogeneity in the streamwise direction.

Judging from the a priori tests and the balance of the Reynolds stress transport equation, the pressure-strain rate term provides the most severe modelling difficulties. While a relatively accurate description of the dissipation rate tensor can be obtained with not too complex means of modelling, the response of the pressure-strain rate tensor to a wide range of rotation rates is difficult to capture. Of the tested models, the SJ-model makes the best overall predictions. The WJ-CC and SSG-models perform essentially equally well/bad. It should be mentioned that none of the formulations include any sort of explicit near-wall modifications. The SJ-model was, however, derived by considering realizability enabling the model to correctly capture the two-component limit at the wall, and hence give a good behaviour in the near-wall region. Furthermore, the SJ-model has been calibrated by using data from direct numerical simulations of nonrotating channel flow. From this point of view the comparison can be argued not to be fair. It should also be remembered that in a RANS-closure the accuracy of the length-scale determining quantity plays a crucial role. This problem is perhaps of more fundamental nature in RANS-closures than the modelling of the individual components of the Reynolds stress transport equation. It is therefore not guaranteed that good predictions are obtained when a model which gives accurate a priori predictions is applied in a general RANS-based flow solver. Still, a sound procedure for developing RANS-closures should be to, as accurately as possible, model the various terms of the considered transport equations and then, if necessary, make the necessary "error-cancelling" adjustments.

In the present study, the pressure-strain rate term has been divided into a rapid and a slow part according to the formal split of the fluctuating pressure, see e.g. Hallbäck et al. [15]. While the rapid pressure-strain part of a particular model is unambiguous due to its direct dependency on the mean velocity gradients, the division between the slow pressure-strain and dissipation rate models is somewhat arbitrary. Speziale et al. [12] proposed the use of an isotropic model for the dissipation rate tensor. This has been adopted in the present study, for both the SSG and CC-WJ models. This is important to remember since both the SSG and CC-WJ models are calibrated as a whole, including models also for the dissipation rate (anisotropy) tensor. From this point of view, the present a priori tests for the slow part of the pressure-strain and dissipation rate tensors should be taken with caution when considering the predictive capability of a particular complete model.

The rapid pressure-strain rate representation derived with the least-squares method is useful for studying the ideal behaviour of the model coefficients, especially since the representation derived is exact for two dimensional mean flows, and hence also for the particular case of rotating channel flow. However, the outcome clearly demonstrates the difficulties of developing a tensorially linear model that gives the correct behaviour for a wide range of rotation rates. The shift in some of the underlying C-parameters for increased rotation rates as well as the interpretation of the behaviour on the stable side must be carefully considered. It should, however, be pointed out that, for $Re_\tau = 180$, the plot corresponding to Fig. 7(a) shows a very similar behaviour compared to the $Re_\tau = 360$ case. This indicates that the Reynolds number is of less importance away from the wall, at least for the present Reynolds number regime.

For modelling purposes, preferably invariant scalar quantities with a local spatial dependence should be used. This includes, for instance, invariants formed from the mean velocity gradients and the Reynolds stress anisotropy. From this point of view the two-componentiality function, defined as $F = 1 - 9(II_{\mathbf{a}} - III_{\mathbf{a}})/8$ where $II_{\mathbf{a}}$ and $III_{\mathbf{a}}$ are the second and third invariants of $\mathbf{a}$, is useful. F is unity for isotropic turbulence and zero at the two-component limit, i.e. at the wall, and could hence be used to capture, e.g., the behaviour of β_1 or $\beta_1^{(s)}$ seen in Fig. 8. In fact, this is exactly what Sjögren and Johansson [1] realized, see (51) in Appendix A. Similar applications of F for the rapid pressure-strain can be considered. For the present case, the commonly used Van-Driest type of damping function can, with the correct calibration, be used in correspondence with F. This, however, implies a dependence on the wall-normal distance. The "two-componentiality" approach is relieved of this difficulty.

Other flows that could be interesting to study using the least-squares based optimization approach include fully developed rotating turbulent pipe flow, boundary layer flows and, of course, flows with separation. A study including several flow cases and Reynolds numbers is very attractive since trends and behaviours of the coefficients of different model forms could be investigated and compared. This has partly been done in the present study, but not to the extent to give any general impact on turbulence closures. The main purpose of the present study should instead be to demonstrate the modelling difficulties of rotating flows as well as to introduce the least-squares method as a useful tool for model development.

Appendix A. The Sjögren–Johansson model in short

The differential Reynolds stress model proposed by Sjögren and Johansson [1], SJ-DRSM, is described in short below. For full details see Sjögren and Johansson [1]. The pressure-strain rate model is divided into two parts, rapid and slow. The tensorial expression for the rapid part is given by

$$\frac{\boldsymbol{\Pi}^{(r)}}{\varepsilon} = (q_1 I_{\mathbf{aS}} + q_9 I_{\mathbf{aaS}})\mathbf{a} + q_2\mathbf{S} + q_3\left(\mathbf{aS} + \mathbf{Sa} - \frac{2}{3}I_{\mathbf{aS}}\mathbf{I}\right) + q_4(\mathbf{a}\boldsymbol{\Omega} - \boldsymbol{\Omega}\mathbf{a}) + (q_5 I_{\mathbf{aS}} + q_{10} I_{\mathbf{aaS}})\left(\mathbf{a}^2 - \frac{1}{3}II_{\mathbf{a}}\mathbf{I}\right) + q_6\left(\mathbf{aSa} - \frac{1}{3}I_{\mathbf{aaS}}\mathbf{I}\right) + q_7\left(\mathbf{a}^2\boldsymbol{\Omega} - \boldsymbol{\Omega}\mathbf{a}^2\right) + q_8\left(\mathbf{a}^2\boldsymbol{\Omega}\mathbf{a} - \mathbf{a}\boldsymbol{\Omega}\mathbf{a}^2\right) \tag{26}$$

in which $I_{\mathbf{aS}} = \{\mathbf{aS}\}$ and $I_{\mathbf{aaS}} = \{\mathbf{aSS}\}$. Note that $\mathbf{S}$ and $\boldsymbol{\Omega}$ are nondimensionalized by $\tau = K/\varepsilon$. In (26), the q-parameters can have a dependence on the invariants of the Reynolds stress tensor anisotropy. Sjögren and Johansson [1] deduced that a model for the rapid pressure-strain rate tensor based on (26), truncated at fifth order have the following parameters

$$q_2 = \frac{4}{5} - \frac{1}{10}(4q_1 - 3q_7)II_{\mathbf{a}} - \frac{2}{5}q_9 III_{\mathbf{a}}, \tag{27}$$

$$q_3 = \frac{12}{7} + \frac{9}{7}q_4 - \frac{1}{7}(3q_8 + 2q_9)II_{\mathbf{a}} - \frac{2}{7}q_{10}III_{\mathbf{a}}, \tag{28}$$

$$q_5 = q_9, \tag{29}$$

$$q_6 = 6q_1 - 9q_7 - q_{10}II_{\mathbf{a}} \tag{30}$$

which in turn depend on

$$q_4 = \eta_1 + \eta_4 II_{\mathbf{a}} + \eta_7 III_{\mathbf{a}} + \eta_{11} II_{\mathbf{a}}^2,$$

$$q_1 = \eta_2 + \eta_8 II_{\mathbf{a}} + \eta_{12} III_{\mathbf{a}}, \qquad q_7 = \eta_3 + \eta_9 II_{\mathbf{a}} + \eta_{13} III_{\mathbf{a}},$$

$$q_8 = \eta_5 + \eta_{14} II_{\mathbf{a}}, \qquad q_9 = \eta_6 + \eta_{15} II_{\mathbf{a}}, \qquad q_{10} = \eta_{10}.$$

For the fifth order model, the generalized realizability condition, see Johansson and Hallbäck [26], implies that 8 of the 15 η-parameters are determined yielding

$$\eta_7 = \frac{39}{40} + \frac{9}{8}\eta_1 + \frac{7}{20}\eta_6 - \frac{1}{6}\eta_{10}, \tag{31}$$

$$\eta_8 = -\frac{495}{112} - \frac{513}{112}\eta_1 - \frac{9}{8}\eta_2 - \frac{57}{14}\eta_4 + \frac{19}{14}\eta_5 - \frac{19}{28}\eta_6 + \frac{1}{3}\eta_{10}, \tag{32}$$

$$\eta_9 = -\frac{423}{112} - \frac{459}{112}\eta_1 - \frac{9}{8}\eta_3 - \frac{51}{14}\eta_4 + \frac{17}{14}\eta_5 - \frac{17}{28}\eta_6 + \frac{1}{6}\eta_{10}, \tag{33}$$

$$\eta_{11} = -\frac{351}{224} - \frac{405}{224}\eta_1 - \frac{45}{28}\eta_4 + \frac{39}{112}\eta_5 - \frac{51}{112}\eta_6 + \frac{1}{8}\eta_{10}, \tag{34}$$

$$\eta_{12} = \frac{9}{20} + \frac{9}{8}\eta_2 - \frac{3}{8}\eta_5 - \frac{27}{40}\eta_6 + \frac{1}{4}\eta_{10}, \tag{35}$$

$$\eta_{13} = \frac{9}{40} + \frac{9}{8}\eta_3 - \frac{3}{8}\eta_5 - \frac{21}{40}\eta_6 + \frac{1}{4}\eta_{10}, \tag{36}$$

$$\eta_{14} = -\frac{351}{56} - \frac{405}{56}\eta_1 - \frac{45}{7}\eta_4 + \frac{39}{28}\eta_5 - \frac{51}{28}\eta_6 + \frac{1}{2}\eta_{10}, \tag{37}$$

$$\eta_{15} = -\frac{351}{112} - \frac{405}{112}\eta_1 - \frac{45}{14}\eta_4 + \frac{39}{56}\eta_5 - \frac{51}{56}\eta_6 + \frac{1}{4}\eta_{10}. \tag{38}$$

The corresponding fourth order model is obtained by setting

$$\eta_1 = -\frac{28}{3}\gamma_1 - \frac{4}{3}, \tag{39}$$

$$\eta_2 = -8\gamma_2 + 36\gamma_3, \tag{40}$$

$$\eta_3 = -16\gamma_2 + 28\gamma_3, \tag{41}$$

$$\eta_4 = -\frac{9}{40} + \frac{21}{2}\gamma_1 - \frac{228}{5}\gamma_2 - 17\gamma_3 + \frac{2}{9}\gamma_4, \tag{42}$$

$$\eta_5 = -\frac{3}{2} - 132\gamma_2 + \frac{2}{3}\gamma_4, \tag{43}$$

$$\eta_6 = \frac{3}{2} + 60(\gamma_2 + \gamma_3), \qquad \eta_{10} = \gamma_4 \tag{44}$$

which, hence, has four undetermined parameters. This model has been used in the present computations in conjunction with the parameter values proposed by Sjögren and Johansson [1], $\gamma_1 = -0.075$, $\gamma_2 = -0.0115$, $\gamma_3 = -0.05$ and $\gamma_4 = -2.1$.

In Sjögren and Johansson [1] there is a misprint in the γ-parameters specifying the second and third order models. The correct expressions, for the third order model, read

$$\gamma_2 = -\frac{3}{88} - \frac{5}{11}\gamma_1, \qquad \gamma_3 = \frac{3}{88} + \frac{21}{22}\gamma_1, \qquad \gamma_4 = 0, \tag{45}$$

and for a second order model

$$\gamma_1 = -\frac{1}{20}, \qquad \gamma_2 = -\frac{3}{88} - \frac{5}{11}\gamma_1, \tag{46}$$

$$\gamma_3 = \frac{3}{88} + \frac{21}{22}\gamma_1, \qquad \gamma_4 = 0, \tag{47}$$

hence, the third order model has one undetermined parameter while all parameters are determined for the second order model.

The nonlinear (optional) extensions of the rapid pressure-strain rate model are given by

$$\mathbf{N}^{\boldsymbol{\Omega}} = \frac{1}{\sqrt{-II_{\boldsymbol{\Omega}}}}\left(\mathbf{a}\boldsymbol{\Omega}^2 + \boldsymbol{\Omega}^2\mathbf{a} - \frac{2}{3}\{\mathbf{a}\boldsymbol{\Omega}^2\}\mathbf{I}\right), \tag{48}$$

$$\mathbf{N}^{\mathbf{S}} = \frac{1}{\sqrt{II_{\mathbf{S}}}}\left(\mathbf{a}\mathbf{S}^2 + \mathbf{S}^2\mathbf{a} - \frac{2}{3}\{\mathbf{a}\mathbf{S}^2\}\mathbf{I}\right) \tag{49}$$

(48) and (49) uses the same model coefficient $C_\Omega = 0.5$.

The models for the slow pressure-strain and dissipation rate tensors are given by

$$\frac{\boldsymbol{\Pi}^{(s)}}{\varepsilon} = f(Re_T)\left(\beta_1\mathbf{a} + \beta_2\left(\mathbf{a}^2 - \frac{1}{3}II_\mathbf{a}\mathbf{I}\right)\right), \tag{50}$$

$$\boldsymbol{\varepsilon} = \varepsilon\left((1 + a_1' F)\mathbf{a} + a_2 F\left(\mathbf{a}^2 - \frac{1}{3}II_\mathbf{a}\mathbf{I}\right)\right) + \frac{2}{3}\varepsilon\mathbf{I}, \tag{51}$$

where

$$f(Re_T) = -\frac{C_\infty}{c_1}\left(\sqrt{2\frac{Re_T}{R_b} + \left(\frac{Re_T}{R_b}^2\right)^2} - \frac{Re_T}{R_b}\right), \tag{52}$$

$$\beta_1 = c_1 F + \left(\frac{9}{8}c_1 + c_3\right)\left(\frac{8}{9}(F-1) + 2II_\mathbf{a} - II_\mathbf{a}^2\right), \tag{53}$$

$$\beta_2 = c_2 F + \left(\frac{9}{8}c_1 + c_3\right)\left(\frac{1}{2}II_\mathbf{a} + \frac{3}{2}III_\mathbf{a}\right). \tag{54}$$

The model parameters $a_1' = -0.5$, $a_2 = 0.0$, $c_1 = -2.4$, $c_2 = 2.2$, $c_3 = 1.2$, $R_b = 1300$ and $C_\infty = 2.58$ were set in accordance with Sjögren and Johansson [1]. The function F is defined as

$$F = 1 - \frac{9}{8}(II_\mathbf{a} - III_\mathbf{a}) \tag{55}$$

and has a range of $0 \leqslant F \leqslant 1$. F is unity for isotropic turbulence and zero at the two-component limit.

Appendix B. Least-squares representation coefficients

This appendix describes the representation coefficients for a general traceless and symmetric second rank tensor, e.g. rapid/slow pressure-strain rate, obtained with the least-squares method for a set of three, two or one basis tensors. The representation using three basis tensors, $\tilde{\boldsymbol{\Pi}}$, is on the form

$$\tilde{\boldsymbol{\Pi}} = \varepsilon\left(c_2\mathbf{B}^{(2)} + c_3\mathbf{B}^{(3)} + c_4\mathbf{B}^{(4)}\right), \tag{56}$$

where $\mathbf{B}^{(2,3,4)}$ are independent basis tensors and $\boldsymbol{\Pi}$ (no tilde) is the exact form of the tensor to be represented. The coefficients are derived through a least-squares procedure in which the last step involves solving the linear system of equations given by

$$\sum_{k=2}^{4} c_k\left\{\mathbf{B}^{(k)}\mathbf{B}^{(p)}\right\} = \left\{\boldsymbol{\Pi}\mathbf{B}^{(p)}\right\}, \quad j = 2, 3, 4, \tag{57}$$

where $\{\cdot\}$ denotes the trace. Solving (57) for c_k gives

$$\begin{aligned} c_2 = {} & \left(\left\{\mathbf{B}^{(2)}\mathbf{B}^{(2)}\right\}\left\{\mathbf{B}^{(3)}\mathbf{B}^{(3)}\right\}\left\{\boldsymbol{\Pi}\mathbf{B}^{(4)}\right\} - \left\{\mathbf{B}^{(2)}\mathbf{B}^{(2)}\right\}\left\{\mathbf{B}^{(3)}\mathbf{B}^{(4)}\right\}\left\{\boldsymbol{\Pi}\mathbf{B}^{(3)}\right\}\right. \\ & - \left\{\mathbf{B}^{(2)}\mathbf{B}^{(3)}\right\}^2\left\{\boldsymbol{\Pi}\mathbf{B}^{(4)}\right\} + \left\{\mathbf{B}^{(2)}\mathbf{B}^{(3)}\right\}\left\{\boldsymbol{\Pi}\mathbf{B}^{(2)}\right\}\left\{\mathbf{B}^{(3)}\mathbf{B}^{(4)}\right\} \\ & \left. + \left\{\mathbf{B}^{(2)}\mathbf{B}^{(4)}\right\}\left\{\mathbf{B}^{(2)}\mathbf{B}^{(3)}\right\}\left\{\boldsymbol{\Pi}\mathbf{B}^{(3)}\right\} - \left\{\mathbf{B}^{(2)}\mathbf{B}^{(4)}\right\}\left\{\boldsymbol{\Pi}\mathbf{B}^{(2)}\right\}\left\{\mathbf{B}^{(3)}\mathbf{B}^{(3)}\right\}\right)/(\varepsilon dd), \end{aligned} \tag{58}$$

$$\begin{aligned} c_3 = {} & \left(\left\{\mathbf{B}^{(2)}\mathbf{B}^{(2)}\right\}\left\{\boldsymbol{\Pi}\mathbf{B}^{(3)}\right\}\left\{\mathbf{B}^{(4)}\mathbf{B}^{(4)}\right\} - \left\{\mathbf{B}^{(2)}\mathbf{B}^{(2)}\right\}\left\{\mathbf{B}^{(3)}\mathbf{B}^{(4)}\right\}\left\{\boldsymbol{\Pi}\mathbf{B}^{(4)}\right\}\right. \\ & - \left\{\mathbf{B}^{(2)}\mathbf{B}^{(3)}\right\}\left\{\boldsymbol{\Pi}\mathbf{B}^{(2)}\right\}\left\{\mathbf{B}^{(4)}\mathbf{B}^{(4)}\right\} + \left\{\mathbf{B}^{(2)}\mathbf{B}^{(3)}\right\}\left\{\boldsymbol{\Pi}\mathbf{B}^{(4)}\right\}\left\{\mathbf{B}^{(2)}\mathbf{B}^{(4)}\right\} \\ & \left. + \left\{\mathbf{B}^{(2)}\mathbf{B}^{(4)}\right\}\left\{\boldsymbol{\Pi}\mathbf{B}^{(2)}\right\}\left\{\mathbf{B}^{(3)}\mathbf{B}^{(4)}\right\} - \left\{\mathbf{B}^{(2)}\mathbf{B}^{(4)}\right\}^2\left\{\boldsymbol{\Pi}\mathbf{B}^{(3)}\right\}\right)/(\varepsilon dd), \end{aligned} \tag{59}$$

$$\begin{aligned} c_4 = {} & \left(\left\{\boldsymbol{\Pi}\mathbf{B}^{(2)}\right\}\left\{\mathbf{B}^{(3)}\mathbf{B}^{(3)}\right\}\left\{\mathbf{B}^{(4)}\mathbf{B}^{(4)}\right\} - \left\{\boldsymbol{\Pi}\mathbf{B}^{(2)}\right\}\left\{\mathbf{B}^{(3)}\mathbf{B}^{(4)}\right\}^2\right. \\ & - \left\{\boldsymbol{\Pi}\mathbf{B}^{(3)}\right\}\left\{\mathbf{B}^{(2)}\mathbf{B}^{(3)}\right\}\left\{\mathbf{B}^{(4)}\mathbf{B}^{(4)}\right\} + \left\{\boldsymbol{\Pi}\mathbf{B}^{(3)}\right\}\left\{\mathbf{B}^{(2)}\mathbf{B}^{(4)}\right\}\left\{\mathbf{B}^{(3)}\mathbf{B}^{(4)}\right\} \\ & \left. + \left\{\boldsymbol{\Pi}\mathbf{B}^{(4)}\right\}\left\{\mathbf{B}^{(2)}\mathbf{B}^{(3)}\right\}\left\{\mathbf{B}^{(3)}\mathbf{B}^{(4)}\right\} - \left\{\boldsymbol{\Pi}\mathbf{B}^{(4)}\right\}\left\{\mathbf{B}^{(2)}\mathbf{B}^{(4)}\right\}\left\{\mathbf{B}^{(3)}\mathbf{B}^{(3)}\right\}\right)/(\varepsilon dd), \end{aligned} \tag{60}$$

$$dd = \{\mathbf{B}^{(2)}\mathbf{B}^{(2)}\}\{\mathbf{B}^{(3)}\mathbf{B}^{(3)}\}\{\mathbf{B}^{(4)}\mathbf{B}^{(4)}\} - \{\mathbf{B}^{(2)}\mathbf{B}^{(2)}\}\{\mathbf{B}^{(3)}\mathbf{B}^{(4)}\}^2 - \{\mathbf{B}^{(2)}\mathbf{B}^{(3)}\}^2\{\mathbf{B}^{(4)}\mathbf{B}^{(4)}\} \tag{61}$$

$$+ 2\{\mathbf{B}^{(2)}\mathbf{B}^{(3)}\}\{\mathbf{B}^{(2)}\mathbf{B}^{(4)}\}\{\mathbf{B}^{(3)}\mathbf{B}^{(4)}\} - \{\mathbf{B}^{(2)}\mathbf{B}^{(4)}\}^2\{\mathbf{B}^{(3)}\mathbf{B}^{(3)}\}. \tag{62}$$

By following, e.g., Gatski and Jongen [21] it should be clear that the obtained representation coefficients are general in the sense that they provide the least-squares-optimal representation of a tensor, $\boldsymbol{\Pi}$, in terms of the basis tensors $\mathbf{B}^{(k)}$.

A representation based on two basis tensors, $\mathbf{b}^{(1)}$ and $\mathbf{b}^{(2)}$, given by

$$\tilde{\Pi} = \varepsilon\left(\eta_1\mathbf{b}^{(1)} + \eta_2\mathbf{b}^{(2)}\right) \tag{63}$$

can be used for, e.g. the slow pressure strain rate. Solving the corresponding system of equations gives

$$\eta_1 = \frac{\{\boldsymbol{\Pi}\mathbf{b}^{(1)}\}\{\mathbf{b}^{(2)}\mathbf{b}^{(2)}\} - \{\boldsymbol{\Pi}\mathbf{b}^{(2)}\}\{\mathbf{b}^{(1)}\mathbf{b}^{(2)}\}}{\{\mathbf{b}^{(1)}\mathbf{b}^{(1)}\}\{\mathbf{b}^{(2)}\mathbf{b}^{(2)}\} - \{\mathbf{b}^{(1)}\mathbf{b}^{(2)}\}^2}, \tag{64}$$

$$\eta_2 = \frac{\{\boldsymbol{\Pi}\mathbf{b}^{(2)}\}\{\mathbf{b}^{(1)}\mathbf{b}^{(1)}\} - \{\boldsymbol{\Pi}\mathbf{b}^{(1)}\}\{\mathbf{b}^{(1)}\mathbf{b}^{(2)}\}}{\{\mathbf{b}^{(1)}\mathbf{b}^{(1)}\}\{\mathbf{b}^{(2)}\mathbf{b}^{(2)}\} - \{\mathbf{b}^{(1)}\mathbf{b}^{(2)}\}^2}. \tag{65}$$

Similarly, a representation with one basis tensor on the form

$$\tilde{\Pi} = \varepsilon\eta_1^{(s)}\mathbf{b}^{(1)} \tag{66}$$

will have a representation coefficient given by

$$\eta_1^{(s)} = \frac{\{\boldsymbol{\Pi}\boldsymbol{b}^{(1)}\}}{\{\mathbf{b}^{(1)}\mathbf{b}^{(1)}\}}. \tag{67}$$

References

[1] T. Sjögren, A.V. Johansson, Development and calibration of algebraic nonlinear models for terms in the Reynolds stress transport equations, Phys. Fluids 12 (2000) 1554–1572.

[2] R.M.C. So, Y.G. Lai, H.S. Zhang, Second-order near-wall turbulence closures: a review, AIAA J. 29 (1991) 1819–1835.

[3] J. Kim, P. Moin, R. Moser, Turbulence statistics in fully developed channel flow at low Reynolds number, J. Fluid Mech. 177 (1987) 133–166.

[4] B.A. Pettersson, H.I. Andersson, Prediction of longitudinal roll cells in rotating plane turbulent Couette flow, Theor. Comp. Fluid Dyn. 14 (2000) 89–109.

[5] S. Jakirlić, K. Hanjalić, A new approach to modelling near-wall turbulence energy and stress dissipation, J. Fluid Mech. 459 (2002) 139–166.

[6] H.J. Kaltenbach, A priori testing of wall models for separated flows, Phys. Fluids 15 (2003) 3048–3064.

[7] R. Kristoffersen, H.I. Andersson, Direct simulations of low-Reynolds-number turbulent flow in a rotating channel, J. Fluid Mech. 256 (1993) 163–197.

[8] U. Piomelli, J. Liu, Large-eddy simulation of rotating channel flows using a localized dynamic model, Phys. Fluids 7 (1995) 839–848.

[9] E. Lamballais, M. Lesieur, O. Métais, Effects of spanwise rotation on the vorticity stretching in transitional and turbulent channel flow, Int. J. Heat Fluid Flow 17 (1996) 324–332.

[10] K. Alvelius, Studies of turbulence and its modelling through large eddy- and direct numerical simulation, PhD thesis, Department of mechanics, KTH, Stockholm, Sweden, 1999.

[11] J.P. Johnston, R.M. Halleen, D.K. Lezius, Effects of spanwise rotation on the structure of two-dimensional fully developed turbulent channel flow, J. Fluid Mech. 56 (1972) 533–559.

[12] C.G. Speziale, S. Sarkar, T.B. Gatski, Modelling the pressure-strain correlation of turbulence: an invariant dynamical systems approach, J. Fluid Mech. 227 (1991) 245–272.

[13] S. Wallin, A.V. Johansson, An explicit algebraic Reynolds stress model for incompressible and compressible turbulent flows, J. Fluid Mech. 403 (2000) 89–132.

[14] S. Wallin, A.V. Johansson, Modelling streamline curvature effects in explicit algebraic Reynolds stress turbulence models, Int. J. Heat Fluid Flow 23 (2002) 721–730.

[15] M. Hallbäck, A.V. Johansson, A.D. Burden, The basics of turbulence modelling, in: Turbulence and Transition Modelling, Kluwer Academic Publishers, 1996 (Chapter 3).

[16] B.E. Launder, G. Reece, W. Rodi, Progress in the development of Reynolds-stress turbulence closure, J. Fluid Mech. 41 (1975) 537–566.

[17] D. Naot, A. Shavit, M. Wolfstein, Two-point correlation model and the redistribution of Reynolds stresses, Phys. Fluids 16 (1973) 738–743.

[18] A. Lundblad, D.S. Henningson, A.V. Johansson, An efficient spectral integration method for the solution of the Navier–Stokes equations, Tech. Rep., FOI, FFA, SE-16490 Stockholm, Sweden, 1992, 1992-28.

[19] J.C. Rotta, Statistische theorie nichthomogener turbulenz, Z. Angew. Math. Mech. 56 (1951) 219–221.

[20] T. Jongen, T.B. Gatski, General explicit algebraic stress relations and best approximation for three-dimensional flows, Int. J. Eng. Sci. 36 (1998) 739–763.

[21] T.B. Gatski, T. Jongen, Nonlinear eddy viscosity and algebraic stress models for solving complex turbulent flows, Prog. Aerospace Sci. 38 (2000) 655–682.

[22] O. Grundestam, S. Wallin, A.V. Johansson, Techniques for deriving explicit algebraic Reynolds stress model based on incomplete sets of basis tensors and predictions of fully developed rotating pipe flow, Phys. Fluids 17 (2005).
[23] T. Sjögren, A.V. Johansson, Measurement and modelling of homogeneous axisymmetric turbulence, J. Fluid Mech. 374 (1998) 59–90.
[24] J. Weinstock, Theory of pressure-strain rate. Part 2. Diagonal elements, J. Fluid Mech. 116 (1982) 1–29.
[25] O. Grundestam, S. Wallin, A.V. Johansson, Direct numerical simulations of rotating channel flow, J. Fluid Mech., submitted for publication.
[26] A.V. Johansson, M. Hallbäck, Modelling of rapid pressure-strain in Reynolds-stress closures, J. Fluid Mech. 269 (1994) 143–168.